Joint full waveform inversion of early arrivals and reflections: a real OBC case study with gas cloud

W. Zhou[*†], *R. Brossier*[†], *S. Operto*[‡] *and J. Virieux*[†]
[†] *ISTerre, Univ. Grenoble Alpes,* [‡] *Géoazur, CNRS, Univ. Nice Sophia Antipolis,*

SUMMARY

Joint full waveform inversion (JFWI) combines reflection (RWI) and early-arrival (EWI) waveform inversions to build a large-scale velocity model of the subsurface. The misfit function of JFWI requires an explicit separation between the short-spread reflections and the early arrivals, the feasibility of which is illustrated with a real long-offset dataset. Each JFWI iteration is alternated with a waveform inversion/migration of short-spread reflections (IpWI). IpWI provides a short-scale impedance model that is used as an input to build the sensitivity kernel of RWI along the two-way reflection paths. Once a velocity macromodel has been built by JFWI, it can be used as a starting model for classical FWI applied on the full dataset to enrich the high wavenumber content of the subsurface model. We present an application of the above-mentioned workflow to a real 2D OBC profile cross-cutting a gas cloud in the North Sea to review its main promises and pitfalls. Several initial models and offset-driven strategies are assessed with the aim to manage the cycle-skipping issue while producing subsurface models of sufficient vertical and horizontal resolution. Our workflow produces an acceptable FWI velocity model that fits the main early arrivals and reflections when JFWI starts from a smoothed version of an existing traveltime tomography model. Improved scattering-angle illumination provided by the 3D acquisitions should allow us to start the inversion from a crude starting model and would overcome the planar propagation we assume in the 2D geometry.

INTRODUCTION

With the development of long-offset wide-azimuth acquisition geometries, full waveform inversion of early arrivals (EWI) such as diving waves and super-critical reflections is a powerful tool to build an accurate velocity model of the subsurface (Virieux and Operto, 2009). However, one limitation of EWI is related to the penetration of early arrivals in depth, which generally prevents to reach the deepest targeted structure. Moreover, EWI is prone to cycle skipping due to long propagation distances, hence preventing a brute-force application of EWI when very low frequencies are not available. Alternatively, reflection waveform inversion (RWI) (e.g. Xu et al., 2012; Brossier et al., 2015) has been proposed to build the velocity macromodel by restricting the sensitivity kernel of full waveform inversion (FWI) along the two-way transmission paths of short-spread reflections. RWI is alternated with the impedance migration/inversion (IpWI) that produces a short-scale impedance model used as an input to build the RWI sensitivity kernel. A key property of RWI is the significant reduction of cycle-skipping issues through the iterative migration/demigration process embedded in JFWI+IpWI. Due to the different wavepaths involved in EWI and RWI, these two waveform inversions tend to preferentially sample the vertical and horizontal components of the wavenumbers, respectively. This prompts Zhou et al. (2015) to combine EWI and RWI into a joint inversion (JFWI) to increase the wavenumber content of the velocity macromodel and to improve the shallow reconstruction. The JFWI misfit function relies on an explicit separation between early arrivals and short-spread reflections, which might require a careful data preprocessing. Nevertheless, as argued in Wang (2015), sufficiently broadband data are required by RWI to extract the low-wavenumber information from the normal moveout of short-spread reflections. The resulting focused wavelets are suitable to implement the data separation with a simple time window as will be illustrated in this study. In Zhou et al. (2015), we also show with a synthetic experiment that JFWI is immune to cycle skipping as long as a layer-stripping approach is used in which shallow targets are imaged before considering deeper ones.

This study aims to further assess the promises and pitfalls of JFWI with an application on a 2D real OBC dataset collected across a gas cloud in the North Sea. We test different initial models of increasing accuracies and source-receiver offset-driven strategies to assess the sensitivity of the inversion to cycle skipping. The velocity macromodel built by JFWI is further assessed in terms of kinematic accuracy and spatial resolution as an initial model for FWI of the full dataset. Starting from a smoothed version of an existing traveltime tomography model, we succeed in building a velocity model from JFWI followed by FWI that compares reasonably well with an existing 3D FWI model of the area. When we start from a crude 1D initial model, JFWI failed to update enough the low-wavenumber content of the gas cloud, leading to mispositioning of reflectors during FWI. However, an equally good data fit is achieved during both applications, which might suggest that these low wavenumbers lie in the null space of the inverse problem due to the insufficient azimuthal and offset coverage (ill-posedness). This issue would be probably overcome when moving to 3D acquisitions.

METHODOLOGY

Assuming the separability of early arrivals d^e and short-spread reflected d^r data, the weighted misfit function of JFWI can be written as follows

$$C(m) = \frac{1}{2}\|W^e\left(d^e - Ru(m)\right)\|^2 + \frac{1}{2}\|W^r\left(d^r - R\delta u(m,\delta m)\right)\|^2. \quad (1)$$

At each iteration, the wavefield u is computed in the smooth velocity model m whereas the perturbation wavefield δu is computed in the whole model $m+\delta m$ in which the model perturbation δm represents a short-scale impedance model. These two model components are alternatively updated. The operator R samples the modeled wavefields at the receiver positions. The two terms of the misfit function, associated with early arrivals and reflections, preferentially contribute to update the vertical and horizontal components of the low wavenumber

vectors, respectively, and hence are complementary. The explicit separation of these two terms filters out from the model update for m the high-wavenumber single-scattered isochrones generated by the migration of the reflected waves. The footprint of the higher-order isochrones in the model update is mitigated by using the V_P–I_P parametrization, which effectively forces the scale separation between the velocity macromodel and the impedance model (Jannane et al., 1989; Operto et al., 2013).

The overall workflow (Zhou et al., 2015) embeds the following steps from an initial model m_0: [1] Estimate the source wavelet; [2] Least-squares migration of the near-zero offset reflections to generate a new δm parametrized by I_P; [3] JFWI to update m parametrized by V_P; [4] Go back to Step 1 until convergence of Step 3 is achieved. During Step 2, the background component of I_P is kept fixed to its initial value; only δm is updated from the previous V_P update such that traveltimes of zero-offset reflections are still matched during the next V_P update. The computational cost of the JFWI is twice that of FWI but their memory requirement is the same.

DATA PRE-PROCESSING AND MODEL PREPARATION

We apply JFWI to an OBC line acquired in the North Sea. This line lies over a low-velocity gas cloud which generates a strong attenuation of the wavefield (Prieux et al., 2011). The phase and amplitude distortion generated by such attenuation have prevented us to perform reliable acoustic VTI time-domain waveform inversion at frequencies higher than 6Hz.

Fig. 1 shows the recorded data that have been low-pass filtered with 6Hz and 5Hz cut-off frequencies, respectively. The 6Hz data, which have a better signal to noise ratio, are used to control the quality of different initial models that will be discussed later. The 5Hz data are the input data for the inversion throughout this study. From x=8km to 16km, there are a bunch of short-spread reflections from the sediments, the gas cloud and the top of the cap rock. The diving waves from above the gas cloud are recorded over the full offset range as first arrivals. An amplitude high at x=9km (Fig. 1a, red arrow) probably results from a rapid increase of velocity with depth below a 500m depth reflector (Operto et al., 2015). The critical reflection from the cap rock is highlighted by an amplitude high at x=7km (Fig. 1a, blue arrow). The refracted wave from the cap rock with a linear moveout might be recorded as a second arrival between x=1km and x=5km (Fig. 1a, yellow arrow).

To separate the early waves associated to the background model from the short-spread reflections, we apply a time window on the early waves, the starting instant of which is 0 s and the finishing instant is defined by a piece-wise linear function (Fig. 1b, yellow lines):

$$t_{\text{bound}}(h) = \begin{cases} \left(1.59 + \frac{h}{1.608}\right) \text{ s}, & \text{for } h \leq 5\text{km}; \\ 9 \text{ s}, & \text{for } h > 5\text{km}. \end{cases} \quad (2)$$

where h denotes the offset. The rest part of the data outside this time window is considered as short-spread reflections.

Fig. 2a shows a vertical section of a velocity model that was built by 3D reflection traveltime tomography (courtesy of BP). The smooth low-velocity blob in blue represents the gas cloud, which lies above the sharp sediment-cap rock interface at around 2.8km depth. This model allows for a reasonable match of the diving waves up to 8km offsets but is not accurate enough for data fitting at longer offsets (Fig. 3a). To build an initial model for JFWI, we smooth this model with a 2D Gaussian filter (Fig. 2b) such that no apparent reflected waves are generated (Fig. 3b). Besides, we also build a 1D model (Fig. 2c) from the vertical profile of the smoothed model at x=8km to further assess the sensitivity of JFWI to the accuracy of the initial model. At last, the vertical section across the gas cloud of the 3D frequency-domain FWI velocity model developed by Operto et al. (2015) is used as a reference FWI model to assess the velocity models developed in this study (Fig. 2d). It can be checked in Fig. 3d that this reference FWI model allows for the match of all the aforementioned arrivals unlike the three models shown in Fig. 2(a-c) (Fig. 3(a-c)).

WAVEFORM INVERSION RESULTS

Classical FWI

We first show the results of classical FWI applied to the short-offset dataset (offset $<$ 5km) and the full data set starting from the velocity model of Fig. 2b. The FWI results obtained from the full dataset are clearly hampered by cycle skipping of the long-offset early arrivals (Fig. 4a). In contrast, FWI of short-offset data produces a reasonably good velocity model (Fig. 4b) although the long-offset early arrivals computed in this model are not matched (Fig. 4c).

Joint FWI

The velocity and impedance models built by JFWI+IpWI are shown in Fig. 5b,f when the full offset range of early arrivals are used during JFWI with the initial model of Fig. 2b. The resulting velocity model is hampered by cycle skipping as long-offset early arrivals are injected at the beginning of the inversion (Fig. 5f). Compared to the data fit achieved by the initial model (Fig. 3b), the fit at long offsets is improved at the expense of the fit at short offsets (Fig. 6b). The inversion converges to a local minimum as the final velocity model shows an incorrect geometry of the gas cloud and an unrealistic high-velocity bright spot at x=3.5km near the sea bottom (Fig. 5f).

When the 1D model (Fig. 2c) is used as initial model with short-offset data, JFWI successfully focus the lateral ends of the gas cloud but fails to update its low wavenumber content (Fig. 5g). This failure manifests in the impedance image by the mispositioning of the cap-rock reflector (Fig. 5c). However, a good data fit is achieved within the 5km offset range without the evidence of cycle skipping (Fig. 6c). This suggests that the low wavenumbers of the gas cloud can only be updated from longer offset data that contain the critical reflection from the cap rock and the refracted waves from below (Fig. 1, blue and yellow arrows). As expected, these arrivals are not fitted in the seismograms computed in the JFWI model (Fig. 6c).

The velocity and impedance models inferred by JFWI+IpWI using the initial model of Fig. 2b and the short-offset data show the best results (Fig. 5a,e). The gas cloud geometry was refined without the artefacts generated by the inversion of the long-offset early arrivals shown in the JFWI model of Fig. 5f. Compared to the 1D model test, the low wavenumbers that

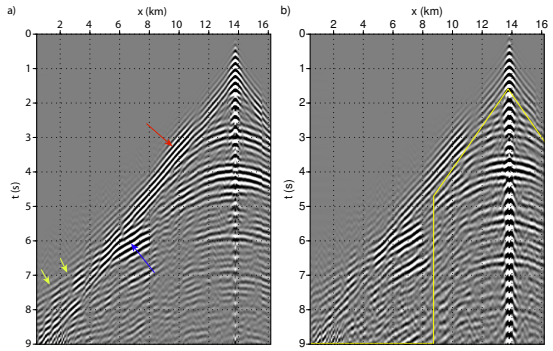

Figure 1: Real data after low-pass filtering below (a) 5Hz and (b) 6Hz. The yellow line indicates the boundary of the time window used to separate the data.

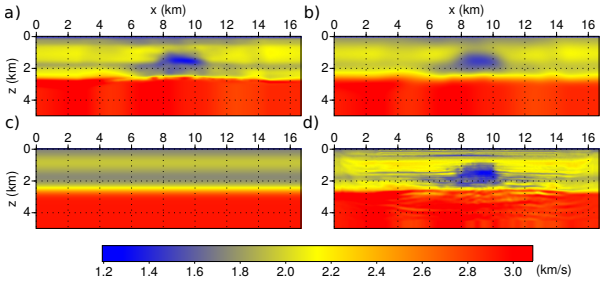

Figure 2: (a) Slice of a 3D velocity model built by reflection traveltime tomography (courtesy of BP). (b) Same as (a) after Gaussian smoothing. (c) 1D velocity model built from the x=8km profile of (b). (d) Slice of the 3D FWI velocity model of. Operto et al. (2015). Velocity models (b-c) are used as initial models for JFWI.

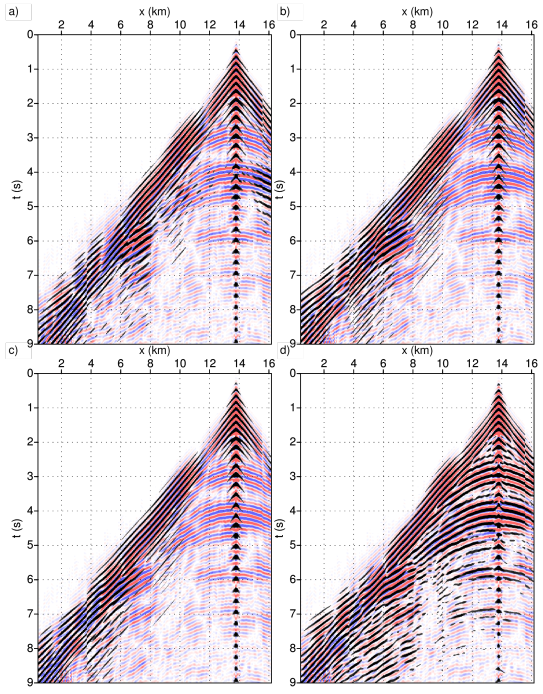

Figure 3: Real data plotted with a blue-white-red scale with superimposed modeled data plotted with a variable area display. Synthetic data are computed in the velocity models shown in Fig. 2. Modeled data are in phase with real data if the black area covers the blue area.

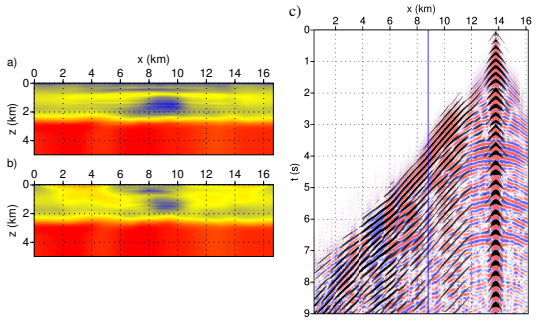

Figure 4: Classical FWI results using (a) short-offset data and (b) the full dataset. (c) Direct comparison between real data (color scale) and modeled data (wiggles) computed in the velocity model shown in (a). Blue line indicates 5km offset. Long-offset data are not matched.

are missing in the JFWI model (Fig. 5g) are to some extent preserved in the initial model of Fig. 2b, which explains why the impedance image in Fig. 5a is more accurate than in Fig. 5c. The good data fit within the 5km offset range is similar to that achieved by the 1D test, while the data fit at long offsets looks better due to the higher low-wavenumber content in the gas cloud (Fig. 6a). This prompts us to proceed with FWI of the full dataset.

Joint FWI followed by Classical FWI

The JFWI model of Fig. 5e is used as an initial model for classical FWI of the full dataset. To prevent cycle skipping, we design an offset-driven strategy in which we gradually increase the offset range starting by 5km maximum offset and ending with the full dataset. The final FWI model is shown in Fig. 5d and the associated data fit is shown in Fig. 6d which presents an improved match at long offsets. The classical FWI increases the resolution of the shallow reflector at 500m depth and succeeds in reconstructing the sharp reflector across the gas cloud at 1.7km depth. These features are consistent with those presented in the reference FWI model (Fig. 2d). However, the JFWI+FWI model of Fig. 5d seems to exhibits a deficit of intermediate wavenumber content above the cap rock relative to the 3D reference FWI model due to the poorer illumination provided by the 2D acquisition geometry.

We apply the same FWI approach starting from the JFWI model inferred from the 1D initial model (Fig. 5g). The final FWI model and the associated seismograms are shown in Figures 5h and 6e. Although the short-scale reflectors are introduced in the FWI model, it still exhibits a deficit of low wavenumbers in the gas cloud leading to overestimated velocities, which result in an incorrect geometry of the reflector cross-cutting the gas cloud at 1.7km depth. However, a data fit similar to Fig. 6e is achieved (Fig. 6d), suggesting that the low-wavenumber content of the gas cloud lies in the null space of the inverse problem defined by the 2D dataset (note the significant difference between the velocity models of Fig. 5d and h). It is likely that a 3D dataset would be beneficial to retrieve these missing lower wavenumbers when JFWI is started from a crude 1D velocity model.

The resolution improvement achieved by FWI (Fig. 5d) relative to JFWI (Fig. 5e) as well as the agreement between the

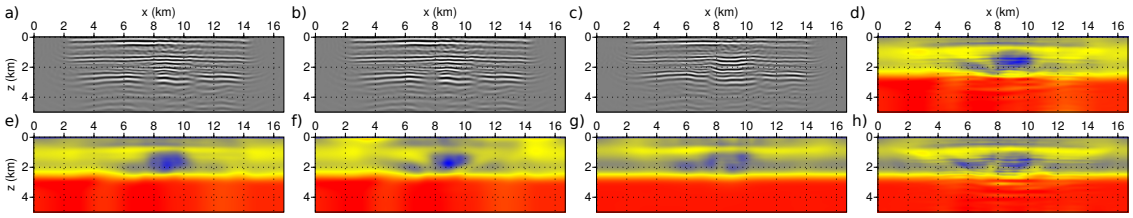

Figure 5: (a,e) JFWI velocity model (e) and impedance model (a) built from short-offset data using the smoothed tomography model of Fig. 2b as initial model. (b,f) Same as (a,e) when early arrivals over the full offset range are used during JFWI. (c,g) Same as (a,e) when the 1D model of Fig. 2c is used as initial model. (d) FWI model using (e) as initial model. (h) FWI model using (g) as initial model.

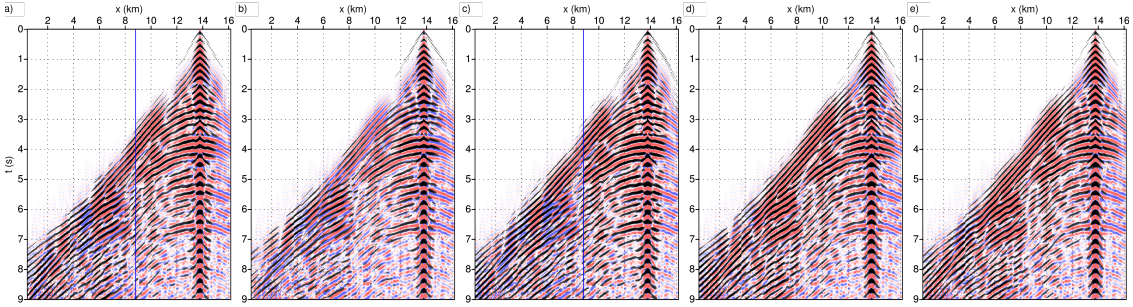

Figure 6: Real data (color scale) versus modeled data (wiggles) computed in the reconstructed velocity models (a,b,c,d,e correspond to Fig 5e,f,g,d,h, respectively). Blue line indicates 5km offset. Note the improved fit on the last two CSGs at far offsets.

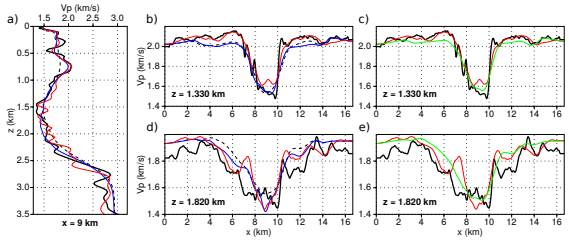

Figure 7: Vertical and horizontal profiles of the reference model (black), the smoothed tomography model (black dashed), the JFWI model (blue), the JFWI+FWI model of Fig. 5d (red), and the FWI model starting from the smoothed tomography model using short offsets (green).

JFWI+FWI model (Fig. 5d) and the reference FWI model are more precisely assessed by the direct comparison of one vertical and two horizontal profiles extracted from these models (Fig. 7a,b,d). In particular, we show the good agreement between the JFWI+FWI model and the reference FWI model down to 1.3km depth. Below this depth, the resolution of the JFWI+FWI model starts degrading, which probably reflects the limited azimuthal and offset coverage of the 2D acquisition geometry. Another reason of these different resolutions may be due to the fact that the sharp reflector at the cap rock level preserved in the reflection traveltime tomography model (Fig. 2a) was not smoothed before FWI in Operto et al. (2015,their figure 7).

To illustrate the benefit of JFWI as an initial model building tool for FWI, profiles of the JFWI+FWI model (Fig. 5d) and the FWI model directly starting from the smoothed model (Fig. 4a) are compared in Fig. 7c,e. Improvement occurs mainly in the horizontal direction, as illustrated between x=3 and 7km at the depth z=1.33km (Fig. 7c) and x=4 to 6km at the depth z=1.82km (Fig. 7e), where the JFWI+FWI model is more consistent with the reference FWI model.

CONCLUSIONS AND PERSPECTIVES

We apply a waveform inversion workflow on 2D long-offset OBC data collected across a gas cloud. This workflow combines early-arrival and reflection waveform inversions with migration/inversion to generate a velocity macromodel that is subsequently used as an initial model for classical FWI. On the one hand, long offsets need to be progressively injected during the latest stages of the workflow to prevent cycle skipping. On the other hand, these long offsets that involve critical reflections and refracted waves from below the gas cloud are also crucial to update the low wavenumbers in the gas cloud, which have a strong impact on the kinematic accuracy of the subsurface model. The workflow combining JFWI, IpWI and classical FWI aims to manage as well as possible the need to prevent cycle skipping while updating the kinematic properties of the subsurface. Perspectives deals with the 3D extension of our workflow to assess whether the extended coverage provided by 3D geometries allows us to relax the need of an accurate velocity model and to improve deep reconstructions, in association with the assessment of possible misfit functions that are more immune to cycle skipping.

ACKNOWLEDGMENTS

This study was partially funded by the SEISCOPE II consortium (*http://seiscope2.osug.fr*). BP, CGG, CHEVRON, EXXON-MOBIL, JGI, PETROBRAS, SAUDI ARAMCO, SCHLUMBERGER, SHELL, SINOPEC, STATOIL, TOTAL and WOODSIDE. We thank BP Norge AS and Hess Norge AS for providing us the data set. This study was granted access to the HPC resources of CIMENT infrastructure (https://ciment.ujf-grenoble.fr) and CINES/IDRIS (allocation 046091 made by GENCI). Authors appreciate discussions with P. L. Yang, P. Wellington and L. Métivier.

EDITED REFERENCES

Note: This reference list is a copyedited version of the reference list submitted by the author. Reference lists for the 2016 SEG Technical Program Expanded Abstracts have been copyedited so that references provided with the online metadata for each paper will achieve a high degree of linking to cited sources that appear on the Web.

REFERENCES

Brossier, R., S. Operto, and J. Virieux, 2015, Velocity model building from seismic reflection data by full waveform inversion: Geophysical Prospecting, **63**, 354–367, http://dx.doi.org/10.1111/1365-2478.12190.

Jannane, M., W. Beydoun, E. Crase, D. Cao, Z. Koren, E. Landa, M. Mendes, A. Pica, M. Noble, G. Roeth, S. Singh, R. Snieder, A. Tarantola, D. Trezeguet, and M. Xie, 1989, Wavelengths of Earth structures that can be resolved from seismic reflection data: Geophysics, **54**, 906–910, http://dx.doi.org/10.1190/1.1442719.

Operto, S., R. Brossier, Y. Gholami, L. Métivier, V. Prieux, A. Ribodetti, and J. Virieux, 2013, A guided tour of multiparameter full waveform inversion for multicomponent data: From theory to practice: The Leading Edge, Special section Full Waveform Inversion, 1040–1054.

Operto, S., A. Miniussi, R. Brossier, L. Combe, L. Métivier, V. Monteiller, A. Ribodetti, and J. Virieux, 2015, Efficient 3-D frequency-domain mono-parameter full-waveform inversion of ocean-bottom cable data: Application to Valhall in the visco-acoustic vertical transverse isotropic approximation: Geophysical Journal International, **202**, 1362–1391, http://dx.doi.org/10.1093/gji/ggv226.

Prieux, V., R. Brossier, Y. Gholami, S. Operto, J. Virieux, O. Barkved, and J. Kommedal, 2011, On the footprint of anisotropy on isotropic full waveform inversion: The Valhall case study: Geophysical Journal International, **187**, 1495–1515, http://dx.doi.org/10.1111/j.1365-246X.2011.05209.x.

Virieux, J., and S. Operto, 2009, An overview of full waveform inversion in exploration geophysics: Geophysics, **74**, no. 6, WCC1–WCC26, http://dx.doi.org/10.1190/1.3238367.

Wang, F., 2015, Waveform inversion based on wavefield decomposition: Ph.D. thesis, l'Ecole nationale supérieure des mines de Paris.

Xu, S., D. Wang, F. Chen, G. Lambaré, and Y. Zhang, 2012, Inversion on reflected seismic wave: 82nd Annual International Meeting, SEG, Expanded Abstracts, 1–7, http://dx.doi.org/10.1190/segam2012-1473.1.

Zhou, W., R. Brossier, S. Operto, and J. Virieux, 2015, Full waveform inversion of diving and reflected waves for velocity model building with impedance inversion based on scale separation: Geophysical Journal International, **202**, 1535–1554, http://dx.doi.org/10.1093/gji/ggv228.